ADVANCING SPOT WELDING PROCESS ASSESSMENT

J. KAARS*, P. MAYR** and K. KOPPE***

*Chemnitz University of Technology, Germany, ORCID 0000-0002-0037-3400, jonny.kaars@mb.tu-chemnitz.de
**Chemnitz University of Technology, Germany, ORCID 0000-0003-2530-4644, peter.mayr@mb.tu-chemnitz.de
***Anhalt University of Applied Sciences, 06366 Koethen/Anhalt, Germany, kurt.koppe@hs-anhalt.de

DOI 10.3217/978-3-85125-615-4-39

ABSTRACT

Resistance spot welding still is one of the most important techniques for joining sheet material. Ongoing developments such as new material grades, coating technologies and process controls generate new challenges for the process. In order to overcome those challenges, numerical process simulation is an important tool in order to develop new welding strategies. Conventional simulation approaches only evaluate basic parameters like nugget diameter, temperature profiles and basic electrical parameters. Although evaluation of these parameters is very important to compare the model to experimental data, it does not do the true evaluation possibilities of numerical models justice.
For the first time, new mathematical methods are presented in this work, which allow the computation of comprehensive parameters like electric potentials, effective temperatures, true electrical resistances and heat contributions as well as mechanical parameters from finite element simulation. Exemplary results of the approach on the example of a spot weld on martensitic 22MnB5 steel are discussed. Among these, for the first time, the quantitative curve of dynamic efficiency of the spot welding process is presented.

Keywords: spot welding, finite element analysis, contact, energy balance

INTRODUCTION

Resistance spot welding (RSW) is perhaps the most important technique for economically joining sheet metal under industrial conditions. Although the process is well-researched, new materials, coatings and methods of process control still create challenges. Two peculiarities characterize RSW: First, the joining heat is generated in the parts to be joined itself, resulting in a strong dependency of the weld heat on material properties of sheets and electrodes. Second, the welding process is covered by the electrodes and the sheets, leaving only external quantities like electrode voltage and –travel accessible to measurements. The difficult relation between welding heat and process conditions in combination with the little measureable data available often makes it hard to further elaborate on the release of the welding heat in terms of location and magnitude. This also holds true even if multiphysical finite-element analyses (FEA) on the process are performed and validated with experiments. The reason is, that conventional FEA computes a spatial distribution of displacement, temperature and electric potential for a number of timesteps, but does not provide preprocessed information on how the temperature distribution evolved. This task

is left to the engineer analysing the data computed. Therefore, unexpected observations on nugget formation in certain welding configurations are often hard to understand and verify.

It is the goal of this work, to provide mathematical methods for further pre-processing of FEA results on RSW. For the first time, this allows enhanced process assessment by means of FEA. The focus lies on deduction of information relevant for the spot welding process from an engineering point-of-view out of the comprehensive amount of spatial data computed with FEA.

DATA ACQUISITION FOR PROCESS ANALYSIS

PRELIMINARIES AND DEFINITIONS

Fig. 1 defines the entirety of mechanical and electrical process quantities accessible to measurement in RSW, along with their location.

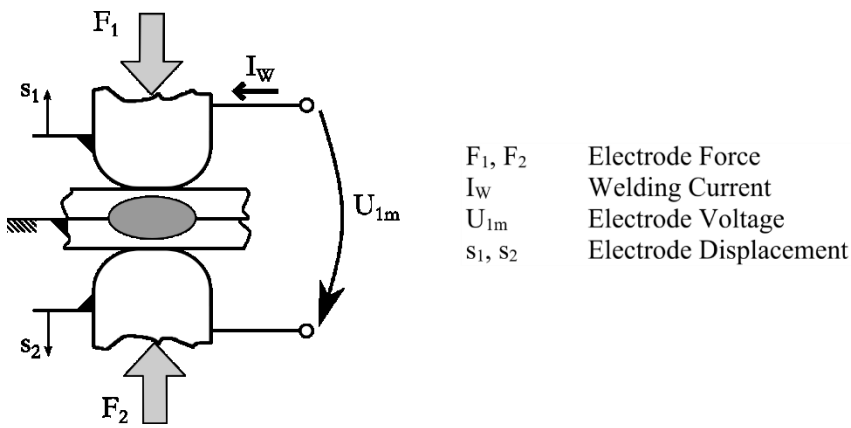

Fig. 1 Process quantities in resistance spot welding.

Usually, the welding current I_w is the main process quantity being adjusted by the machine control. The electrode voltage U_{1m} is the result of the electrical resistance of the weld. It is often recorded for monitoring purposes [1], [2]. While the sheets are clamped together by the electrode forces F_1 and F_2, thermal expansion and softening of the sheets cause a dynamic displacement s_1 and s_2 of the electrodes. The displacement can be used to monitor the process as well, especially to detect splash. In an industrial environment the displacement is difficult to measure, therefore the electrode voltage is preferred in most cases. Each of the quantities needs to be understood as a strong function of time.

The mechanical contact make between sheets and electrodes as well as between the sheets is the most important aspect of a resistance weld, as it defines most of the other quantities. An overview of the situation is given in Fig. 2.

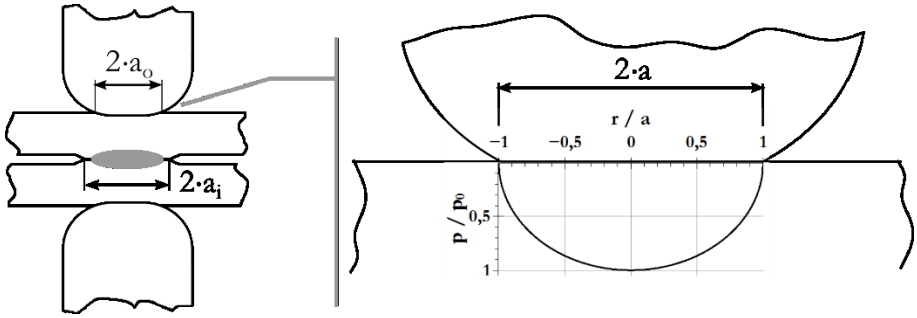

Fig. 2 Mechanical contacts at the weld with an example of the uneven contact pressure distribution according to Hertz‘ [3] theory.

Therein, the contact radii a_i of the inner contact and a_o of the outer contact as introduced by [4] are defined at the weld. That means, the contact area is assumed to be a perfect circle. This will hold true as long as the electrodes are axisymmetric and positioned roughly perpendicular to the sheet surface, i.e. in most practical cases.

In Fig. 2, a representation to scale of the contact pressure distribution at the contact is shown as well. It is important to note, that just like the contact pressure depicted, other quantities at the contact like temperature or electric potential are a more or less strong function of the contact radius as well. In circumferential direction of the contact, the quantities are constant, due to axisymmetry.

The electrical situation during formation of the weld is rather involved, as the electric resistance at the weld needs to be divided into several parts [5]: The bulk resistance of the material and the transition resistance at the contacts. Fig. 3 defines detailed denotations for the resistances and corresponding electric potentials, as well as their localisation.

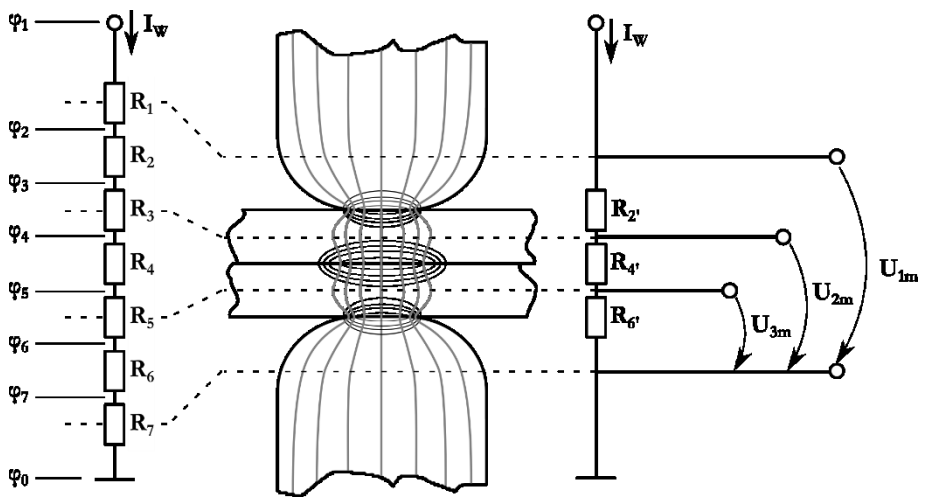

Fig. 3 Definition and location of electrical quantities at the weld, left: true potentials and partial resistances, right: measureable voltages and resistances; illustration by Kaars et al. [6] current flowlines and potential isolines based on Gengenbach [7].

In Fig. 3 on the right, the three partial voltages and their corresponding resistances being measureable during welding are shown. On the left side, the true partial potentials of the

weld and their corresponding resistances are outlined. The dashed lines in between both represent the connection true and measurable resistances and especially their physical location at the weld. The respective true resistance is a

transition resistance for $R_i \quad i \in \{2, 4, 6\}$ (1)

and

bulk resistance for $R_i \quad i \in \{1, 3, 5, 7\}$ (2)

The measureable resistances are composed out of the true resistances by

$$R_i' = R_i + \chi \cdot (R_{i-1}(T) + R_{i+1}(T)) \quad i \in \{2, 4, 6\} \tag{3}$$

with χ being an unknown number fulfilling $0 < \chi < 1$. Each of the true resistances will significantly change its magnitude during the welding process, especially the transition resistance. Most of the dynamic resistance change is driven by temperature [8–11], with the underlying effects being rather complicated. With respect to the scope of this work, the reader shall be pointed to [5], [12], [13] for more details. However, it is important to note, that the resistances are a strong function of time during welding.

Fig. 3 and equation (3) also prove, that it is not possible to determine the true resistance portions, and therefore their respective heat contributions to the weld, by measurements alone. In the following, the enumeration used in Fig. 3, left portion, will also be used to denote other quantities conjoined to the respective locations at the weld.

According to the German Standard DVS 2902-1 [14], a significant part of the total weld heat input is distributed into electrodes and surrounding sheet material, while heat dissipation to the surroundings by radiation and convection can be neglected. The standard states, that in many cases only 10 % of the total heat contributes to the formation of the melt.

A more comprehensive description of the heat flows at the weld is defined in Fig. 4. Therein, the composition of the total welding heat out of its portions, distinguished by heat sources and heat sinks is visualized.

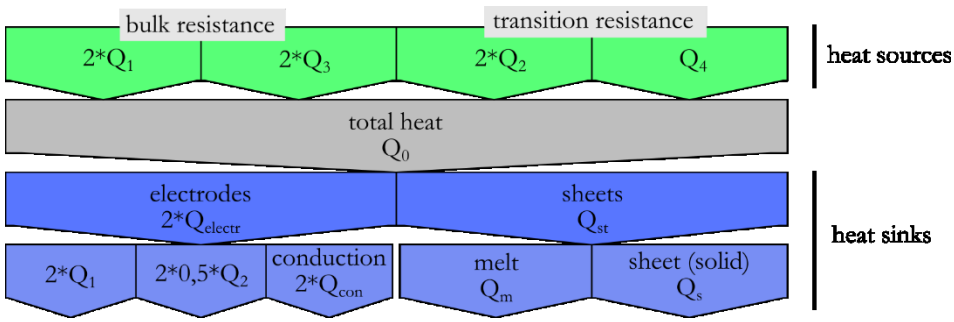

Fig. 4 Definition of the energy flow in a spot weld by heat sources and sinks.

The denomination of the heat sources in Fig. 4 is in accordance with the true resistances R_i in Fig. 3. Moreover, the heat sinks at the weld are divided by their locations, namely electrodes and sheets. The electrode heat Q_{electr} is composed out of heat from its bulk resistance Q_1, half of the transition resistance heat Q_2 and heat conducted into the electrode

from the hot sheet Q_{con}. Depending on the algebraic sign of Q_{con}, the formulation theoretically also allows heating of the sheets by bulk heat from the electrodes. This approach is sometimes used to weld low resistance materials such as copper by using high resistance tungsten or molybdenum electrodes [15]. The heat in the sheets is divided into two portions, one being the melt heat Q_m being stored in the molten zone of the joint, the other being the heat Q_s increasing the temperature of the surrounding sheets. As the melt heat eventually is a portion of the total heat, the description in Fig. 3 is of great relevance for process analysis. By evaluating the different heat portions, one can gather information on where the heat dominantly forming the joint comes from, or why the heat produced does not create a sufficient nugget.

The RSW process features a peculiarity: As soon as the nugget is formed, the melt is exposed to significant hydrostatic pressure caused by the electrode force. Also, this same electrode force causes the unmolten portion of the sheets at the inner contact to be pressed to each other strongly enough in order to ensure secure enclosure of the high-pressure melt. Sometimes this mechanism of melt enclosure fails, resulting in the melt being expulsed out of the weld. This event is known as weld splash or expulsion and is the most important process limit in RSW [16]. In literature, the mechanism of melt enclosure is disputed. Some authors assume that expulsions occur as soon as the molten zone grows larger than the inner contact [17], [18], Broda [19] presumed that excessive melt pressure due to melt evaporation is responsible for the expulsion. Senkara et al. [20] proposed the only mathematical model for splashes available to date. The model assumes splash, as soon as the effective force of the expanding nugget has grown larger than the electrode force. In Fig. 5, a graphical summary of the mechanism of nugget enclosure by contact pressure of the outer contact p_o, with $p_{e,fl}$ being the hydraulic nugget pressure, is shown.

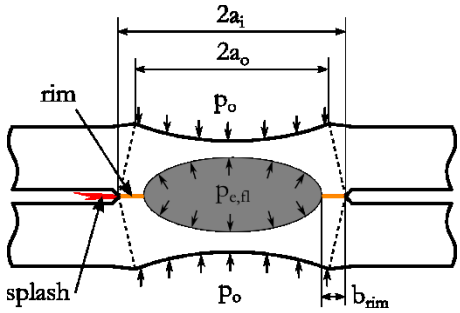

Fig. 5: Enclosure of melt in the spot welding process.

MATHEMATICS OF DATA ACQUISITION

The contact pressure distribution outlined in Fig. 2 is processed to determine the actual contact radii in the FEA: A routine implemented in the postprocessing code evaluates the location of the contact node at which the pressure switches to about zero, starting from the symmetry axis. The contact radii of electrodes and sheets are the most important input quantities for further data processing, as will be shown in the following paragraphs. Of course during the welding process, the contact radii will significantly change their

magnitude, as the sheets will thermally expand and subsequently soften because of the welding heat. This effect is correctly included by the routine, as always the actual contact pressure distribution for the respective timestep is considered for contact radius detection.

Given a quantity $g(r)$ in $0 \leq r \leq a$, also cf. Fig. 2, the space spanned by the curve in the axisymmetric domain can be understood as a volume with the boundaries

$$0 \leq r \leq a \quad \wedge \quad 0 \leq g \leq g(r) \tag{4}$$

According to Guldins second rule [21], the volume of this body of revolution is

$$G = \iint_{(A)} g(r)\, dA = 2\pi \int_0^a g(r) \cdot r\, dr \tag{5}$$

Assumed $g(r)$ for example would represent the contact pressure, then G would be the contact force. As the effective magnitude g_e of $g(r)$ has to have the same physical effect as the unevenly distributed quantity, g_e must fulfil the expression

$$2\pi \int_0^a g_e \cdot r\, dr = 2\pi \int_0^a g(r) \cdot r\, dr \tag{6}$$

which after some transformation yields

$$g_e = \frac{2}{a^2} \int_0^a g(r) \cdot r\, dr \tag{7}$$

However, in FEA the quantity $g(r)$ will never be given as a mathematical function, but as discrete numbers on the respective nodes. For this reason, the integration must be carried out numerically. The approach can also be pictured as a summation of the volumes of a number of hollow cylinders. Equation (5) then can be approximated by

$$G = \sum_{i=1}^{n} G_i \tag{8}$$

$$G_i = 2\pi \cdot \frac{r_i + r_{i-1}}{2} \cdot \frac{g(r_i) + g(r_{i-1})}{2} \cdot (r_i - r_{i-1}) \tag{9}$$

wherein $r_n = a$. Accordingly, the required effective magnitude is written as

$$g_e = \frac{2}{a^2} \cdot \sum_{i=1}^{n} \left(\frac{r_i + r_{i-1}}{2} \cdot \frac{g(r_i) + g(r_{i-1})}{2} \cdot (r_i - r_{i-1}) \right) \tag{10}$$

Expression (10) was implemented into the FEA code to compute the effective magnitude of various quantities in the contact areas, for example effective electric potential, effective pressure and effective temperature. In order to compute the heat content of the molten zone of the sheets, another integration is necessary: At first, all elements whose coldest node of the temperature T_n fulfils the condition $T_n \geq T_m$ are selected. T_m is set by the user fulfilling

$$T_{sol} \leq T_m \leq T_{liq} \tag{11}$$

where T_{sol} is the onset and T_{liq} the end of the sheet materials melting interval. Based on the average temperature $\bar{T}_i$ of the respective element, the heat of the molten zone is written as

$$Q_m = \sum_{i=1}^{k} \left(V_i \cdot h(\bar{T}_i) \right) \tag{12}$$

wherein V_i represents the element volume and $h(\bar{T}_i)$ the specific enthalpy density. Because of the selection approach excluding partially molten elements, the procedure yields the lower limit of the melt heat, but can be slightly adjusted by selection of the melting temperature T_m according to (11).

The criterion (11) was also used in order to detect the nugget diameter in each timestep of the solution. Provided that the inner contact is closed and at least one node in the model supersedes T_m, a postprocessing routine was used to evaluate the nugget diameter. The routine detects the location where the nodal temperature in the inner contact is smaller than T_m for the first time, starting from the symmetry axis.

Computation of Engineering Data

Based on the effective magnitude as described in the preceding section, the effective electric potential φ_i is computed out of the electric potential distribution in each contact surface. This effective potential is the most important prerequisite for caloric considerations at the weld, as it is necessary in order to compute the true resistance contributions at the weld by using the expressions

$$R_i = (\varphi_i - \varphi_{i+1})/I_w \qquad 1 \leq i \leq 6 \tag{13}$$

$$R_7 = \varphi_7/I_w \tag{14}$$

$$R_0 = \varphi_1/I_w \tag{15}$$

Based on those R_i, the heat contributions to the weld result from

$$Q_i = \int_{t_0}^{t_1} R_i(t) \cdot I_w(t)^2 \, dt \qquad 0 \leq i \leq 7 \tag{16}$$

for a welding time from t_0 to t_1. Furthermore, the heat transported across the electrode-sheet contact Q_{con} is computed using expression (9). The local contact heat flow across each contact element therein is considered as $g(r)$ accordingly. Based on these caloric data, the process efficiency can be determined as well. In literature, the terms effective efficiency [22], melt efficiency [23], [24] and process efficiency [24] are defined. Only the effective η_{eff} and melt efficiency η_m shall be discussed here. They are defined as follows:

$$\eta_{eff} = Q_{st}/Q_0 \tag{17}$$

$$\eta_m = Q_m/(\eta_{eff}\, Q_0) \tag{18}$$

Of course, other quantities like local and total electric power, specific transition resistance, effective contact pressure and temperature and many more can be derived using

the data and methods explained above. The latter, along with the electrode heat as defined in Fig. 4, are particularly useful for the evaluation of electrode wear. For the sake of length of this work, these continuative topics shall not be further discussed.

FEA MODEL AND VERIFICATION

With respect to the scope of this work only a brief overview af the model and the experimental conditions used to verify it will be given. The reader shall be pointed to [6], [25–27] for more details. Also, results on the true resistances R_i can be examined in [6].

The FEA model employed for the analysis presented in this work was set up in ANSYS v19, using an axisymmetric model geometry. The elements use a second-order ansatz and have structural, thermal and electrical degrees of freedom. A brief overview over the boundary conditions applied and mesh used is given in Fig. 6. At the inner and outer contacts the model uses the transition resistance model introduced by Kaars et al. [25]. All material properties of the sheets are implemented as functions of temperature up to the melting point.

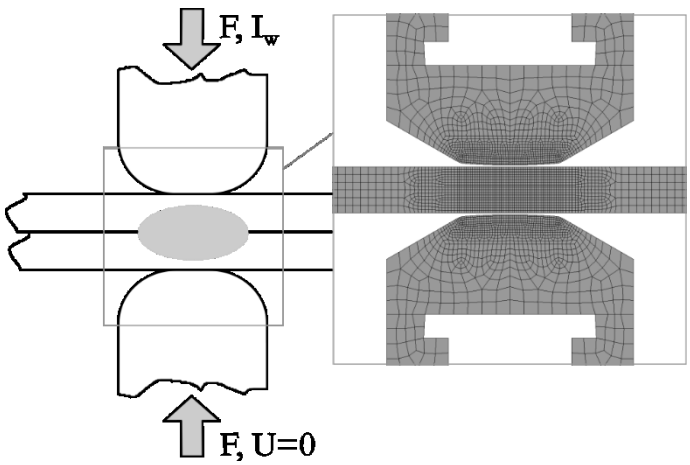

Fig. 6: FEA model, major boundary conditions and mesh.

The FEA was set up to represent welding of two sheets of 1.5 mm martensitic 22MnB5 steel with aluminium-silicon coating AS150. In both, experiments and FEA, a welding force of 6 kN and a welding current up to 6.6 kA were applied.

In welding experiments with an instrumented RSW gun, a data basis was obtained to validate the FEA. Furthermore, the dynamic curve of the resistance R_{1m} was recorded and the result afterwards compared to the computed curve from the FEA. Overall, a very good agreement between both was observed. The reader shall be pointed to [6] for details, more verifying results are presented in the following section. Additionally, the dynamic contact radii and nugget diameter of FEA and experiment were recorded and compared. In order to obtain the data from the experiment, the welding process was prematurely interrupted at certain points. Afterwards, the radius of the electrode indentation a_o was measured using a

microscope Zeiss Axiovert 200. The weld was then mechanically broken open to reveal the nugget and inner contact area, whose radii r_p and a_i were then measured as well.

RESULTS REVIEW AND DISCUSSION

In Fig. 7, the computed and measured results of contact radii and nugget radius are presented. In the contact radii curves, the onset of welding current flow is indicated by a steep decline of both contact radii, especially at the inner contact. The reason for this is the thermal expansion of the sheets in the vicinity of the contacts. As the welding time progresses, the heated sheets begin to soften, which causes the electrodes to sink into the sheets, along with increasing contact radii. It can be readily seen, that the measured values for the contact radii are in good conformity with the computed ones.

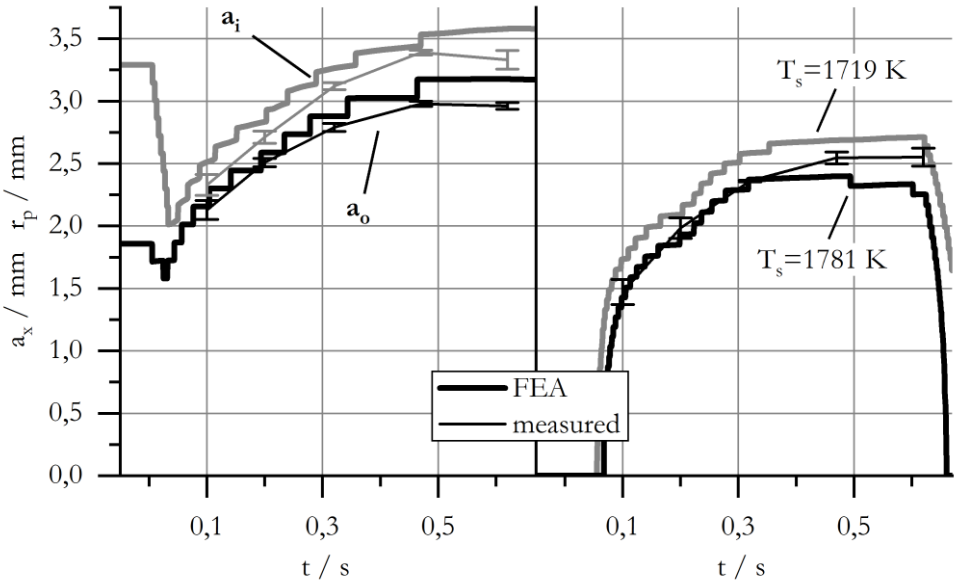

Fig. 7: Comparison of computed and measured dynamic contact radii a_x and nugget radius r_p.

The nugget radius depicted in the right half of the diagram is divided into two curves. At the welded joint, one cannot distinguish for sure at which temperature T_m in the mushy zone with $T_{sol} \leq T_m \leq T_{liq}$ the sheets actually formed a sound joint. But in the FEA, a definition needs to made, at which minimum temperature the joint is considered welded. For this reason, the nugget growth curves are depicted for both limits of the mushy zone. As it can be seen, the deviation between both is small, the measured curve lies well in between. As the dynamic resistance curve of the model conformed very well with the experiments as well, cf. preceding section, the FEA model is considered to be accurate.

In Fig. 8, the distribution of the total welding energy on the individual contributors of the heat sources as well as the heat sinks according to Fig. 4 is shown. It can be seen that the major part of heat generation of about 60 % takes place in the bulk material of the sheets.

The electrode material only contributes roughly 5 %. This is interesting because it also means that about 35 % of the welding heat is released by transition resistances, of which the major part of 30 % is attributed to the outer contacts. About 70 % of the welding heat remains in the electrodes when the weld is finished, with the heat transported into the electrodes by conduction being by far the largest contributor to that amount. About 15 % of the total welding heat in the electrodes is appropriated to the electrical contacts. Obviously, the contact heat distributes itself in equal portions among both contact partners. Only 5 % of the total welding heat are used to form the nugget, while 25 % are used to heat up the sheets around the weld.

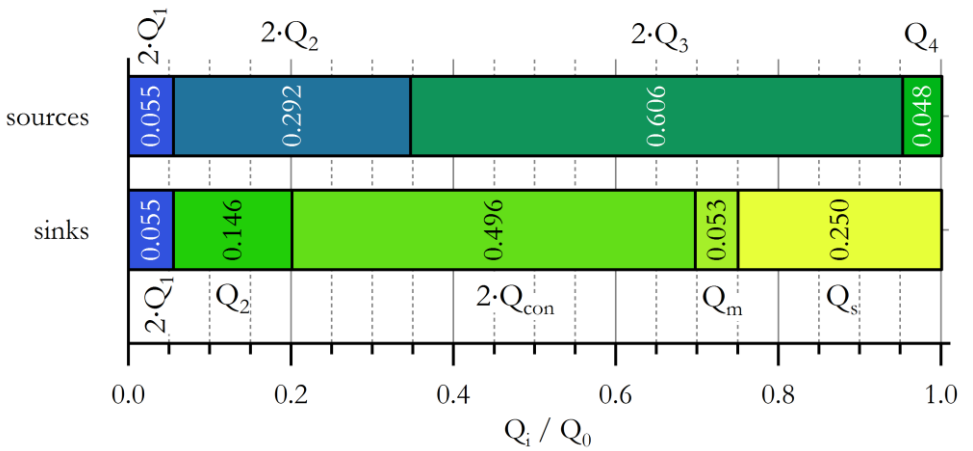

Fig. 8: Relative energy balance at the end of the welding cycle, separated by heat sources and sinks.

The utilization of welding heat for the joint formation can be better observed by evaluating the process efficiencies. Those are depicted in Fig. 9, along with the welding current. It can be seen, that the effective efficiency has its maximum of about 55 % at the very beginning of current flow and from then on decreases to about 30 % at the end of the welding cycle.

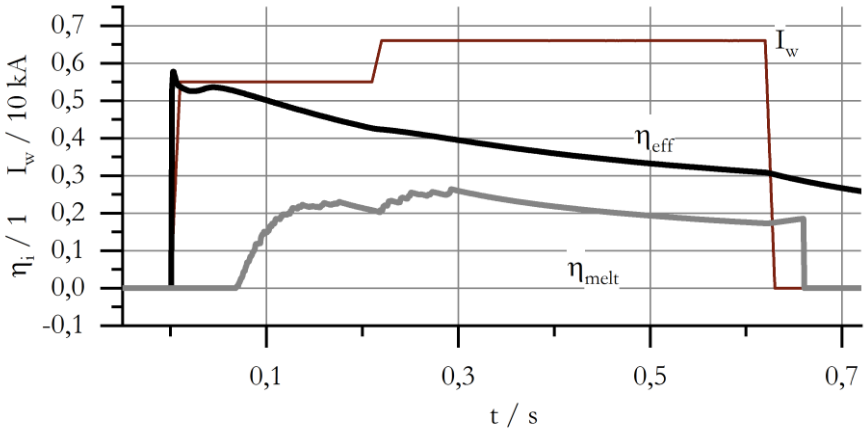

Fig. 9: Dynamic process and melt efficiency of the weld.

The melt efficiency on the contrary has its maximum of about 25 % after about 300 ms after the onset of current flow and decreases to about 18 % towards the end of the welding cycle. These observations have very important consequences: They prove the common assumption, that spot welding is more efficient in terms of relative heat being input into the sheets when the duration of current flow is short [14]. But moreover, they show that a certain duration of current flow exists, at which the energy is utilized best for joint formation. In this case, this happens after about 300 ms of current flow. This instant also coincides with the moment, where nugget formation is practically completed, cf. Fig. 7. Arbitrarily prolonging the welding process over this "optimal welding time" will only decrease efficiency, but not form any more melt volume. Of course, prolonged welding can be advisable for metallurgical reasons in several cases nonetheless.

In Fig. 10, detailed information on the mechanical situation at the inner contact is presented. While therein $T_{e,rim}$ is the effective temperature of the solid rim around the nugget, b_{rim} is the width of the latter, also cf. Fig. 5. Additionally, the hydraulic force exerted by the nugget F_{fl} is displayed as relative portion of the total contact force at the inner contact. Accordingly, $p_{e,rim}$, $p_{e,fl}$ and $p_{e,i}$ are the effective contact pressures of rim, nugget and inner contact in total. Per definition, data on rim and nugget does not exist before the first melt is formed. It can be readily seen, that during the process the rim temperature has a nearly constant temperature of about 200 K below the A_4 point of the sheets. The width of the rim has two maxima of about 2 mm at the end and beginning of the process, while a minimum of about 1 mm exists in the middle of the process. In the same instant where the rim is most narrow, the hydraulic force has its maximum of about 50 % of the inner contact force. The effective pressures all have a maximum at the beginning and from then on decrease hyperbolically. At all times, the fluid pressure in the nugget is the largest pressure, the pressure in the rim the smallest. The effective total pressure lies well in between.

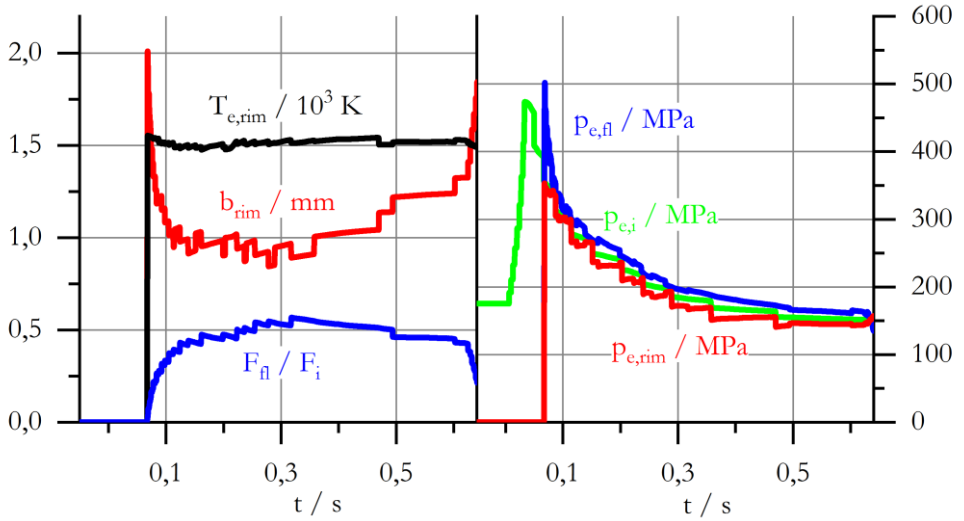

Fig. 10: Dynamic quantities characterizing the enclosure of melt in resistance spot welding.

In Fig. 11, the contact pressure distribution at both contacts of the weld during various stages of the process is displayed. It can be seen, that at both contacts, the contact pressure initially is distributed according to Hertz' theory, cf. Fig. 2. With progress of welding time, the pressure distributions become more and more flattened, especially at the inner contact. At the outer contact, a local maximum of contact pressure forms towards the end of the welding cycle.

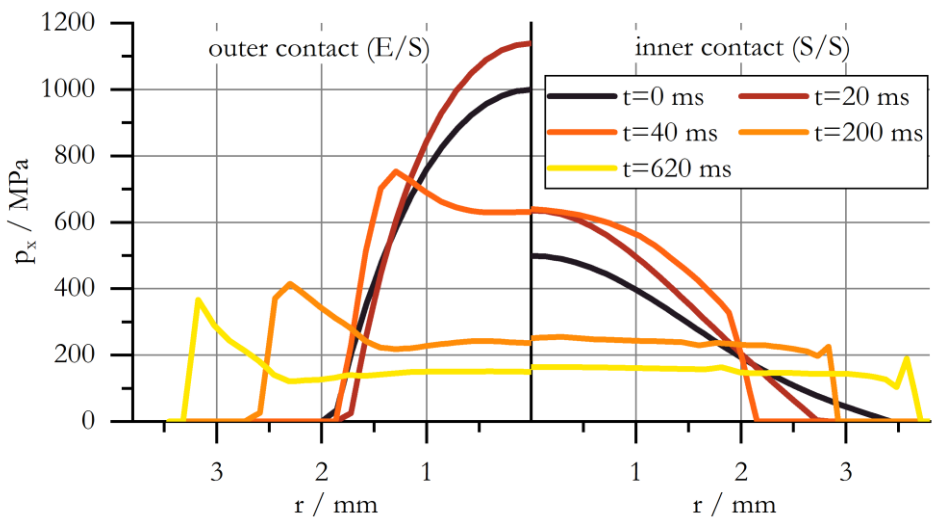

Fig. 11: Contact pressure distribution at the outer (left) and inner (right) contact of the weld during various stages of the welding process.

These information are very important in order to understand the effects responsible for the data in Fig. 10: As the weld advances and the nugget is formed, the sheets soften and

subsequently melt, causing the contact pressure distributions to flatten. This effect is equal to a mechanical representation the effective pressure computation in the contact zone. As a result, the hydraulic pressure in the nugget must be greater than that of the rim at any times, because the hydraulic pressure represents the integration of the high-pressure zone in the middle of the contact. The effective pressure of the contact in total must lie in between that of the melt and that of the rim. This is exactly what is visible in Fig. 10. Fig. 10 also proves, that the width of the rim is not constant at all. Moreover, the conjunction of nugget diameter, rim width and hydraulic melt pressure results in the magnitude of the hydraulic melt force.

These observations have some very important consequences: At first, they prove that a melt pressure greater than that of the rim does not result in a splash, as the rim pressure is the smallest, the melt pressure the greatest pressure at the inner contact at any times anyway. At the very beginning of melting, a melt pressure equal to the maximum contact pressure is present, from that point on the melt pressure can only decrease. Secondly, the hydraulic force of the melt can never exceed the inner contact force, as long as a rim exists. In case of total melting of the rim, the relative hydraulic force would be one. Of course melting of the rim would result in a splash anyway. That means, that splashes can't be a result of the hydraulic force getting larger than the electrode force.

CONCLUSIONS

The FEA model presented has been proven capable of accurately computing the nugget diameter as well as the contact radii of an exemplary weld of martensitic steel. Methods have been introduced, to extend the assessment of the computed data by important process parameters such as resistances, energies, efficiencies as well as mechanical pressures and forces. The method is extendable to other potential quantities of interest.

For the first time, a comprehensive quantitative energy balance of the spot welding process for heat sources as well as heat sinks has been computed using the methods outlined. Additionally, the dynamic curve of effective and melt efficiency have been computed for the first time.

The data suggests, that an optimal duration of current flow in resistance spot welding may exist. Furthermore, the computed parameters proved, that the hydraulic pressure in the nugget is larger than that of the surrounding rim at any time. That means, that increased nugget pressure as assumed in literature can't be a reason for welding splashes. This indirectly also means, that the force exerted by the molten nugget will never exceed the electrode force.

REFERENCES

[1] N., N.: *Untersuchung innovativer Geräte zur Qualitätssicherung beim Widerstandspunktschweißen* (Forschungsbericht Nr. AiF-13.568N). München : SLV München, 2005

[2] MIRO, URAN: *Qualitätsüberwachung beim Widerstandspunktschweißen mittels mehrparametrischer Analyse*. Berlin, Technische Universität Berlin, Dissertation, 2004

[3] HERTZ, HEINRICH: Über die Berührung fester elastischer Körper. In: *Journal of Engineering Materials and Technology* Bd. 92 (1881)
[4] HOLM, RAGNAR: *Die technische Physik der elektrischen Kontakte*. 1. Aufl. Berlin : Springer-Verlag, 1941
[5] BRUNST, WALTER: *Das elektrische Widerstandsschweißen*. 1. Aufl. Berlin : Springer-Verlag, 1952
[6] KAARS, J. ; KOPPE, K. ; GEORGI, W. ; MAYR, P.: Transition resistance of 22MnB5+AS150—experimental results and their numerical application. In: *Welding in the World* (2017)
[7] GENGENBACH, O.: Untersuchungen über die Stromverteilung, den Wärmefluss und die Temperaturverteilung in der Umgebung von Widerstandsschweißpunkten. In: *Schweißtechnik* Bd. 45 (1965)
[8] ROGEON, P. ; CARRE, P. ; COSTA, J. ; SIBILIA, G. ; SAINDRENAN, G.: Characterization of electrical contact conditions in spot welding assemblies. In: *Journal of Materials Processing Technology* Bd. 195 (2008), Nr. 1–3
[9] RAOELISON, R.N. ; FUENTES, A. ; POUVREAU, C. ; ROGEON, PH. ; CARRÉ, P. ; DECHALOTTE, F.: Modeling and numerical simulation of the resistance spot welding of zinc coated steel sheets using rounded tip electrode: Analysis of required conditions. In: *Applied Mathematical Modelling* Bd. 38 (2014), Nr. 9–10
[10] ESHRAGHI, MOHSEN ; TSCHOPP, MARK A. ; ASLE ZAEEM, MOHSEN ; FELICELLI, SERGIO D.: Effect of resistance spot welding parameters on weld pool properties in a DP600 dual-phase steel: A parametric study using thermomechanically-coupled finite element analysis. In: *Materials & Design* Bd. 56 (2014)
[11] GESLAIN, EDOUARD ; ROGEON, PHILIPPE ; PIERRE, THOMAS ; POUVREAU, CÉDRIC ; CRETTEUR, LAURENT: Coating effects on contact conditions in resistance spot weldability. In: *Journal of Materials Processing Technology* Bd. 253 (2018)
[12] HOLM, RAGNAR: *Electric Contacts - Theory and Application*. 4. Aufl. : Springer-Verlag, 1967. — 3. Reprint der 4. Aufl. von 1967
[13] JOHNSON, K.L.: *Contact Mechanics*. Cambridge : Cambridge University Press, 1987. — Ninth Printing 2003
[14] DVS-MERKBLATT 2902-1: *Widerstandspunktschweißen von Stählen bis 3mm Einzeldicke - Übersicht*
[15] N., N.: *Schweißen von Kupfer und Kupferlegierungen* (Informationsschrift) : Deutsches Kupferinstitut, 2009
[16] NORM DIN EN ISO 14327: *Widerstandsschweißen - Verfahren für das Bestimmen des Schweißbereichsdiagramms für das Widerstandspunkt-, Buckel- und Rollennahtschweißen*, 2004
[17] SHEN, J. ; ZHANG, Y. S. ; LAI, X. M.: Influence of initial gap on weld expulsion in resistance spot welding of dual phase steel. In: *Science and Technology of Welding and Joining* Bd. 15 (2010), Nr. 5
[18] NIELSEN, CHRIS VALENTIN: *Genzbedingung für die Spritzerentstehung*. Aachen, SWANTEC Software and Engineering ApS, pers. Mitteilung, 2013
[19] BRODA, TOBIAS: Pulsierender Gleichstrom für Blechdickenkombinationen. In: *16. Kolloquium Widerstandsschweißen und alternative Verfahren*. Halle/Saale, 2014
[20] SENKARA, J. ; ZHANG, H. ; HU, S. J.: Expulsion Prediction in Resistance Spot Welding. In: *Welding Journal* (2004), Nr. 04
[21] PAPULA, LOTHAR: *Mathematik für Ingenieure und Naturwissenschaftler*, *Studium*. Bd. 2. 12. Wiesbaden : Vieweg + Teubner, 2009
[22] SCHELLHASE, MARTIN: *Der Schweißlichtbogen – ein technologisches Werkzeug*. Berlin : Verlag Technik, 1985
[23] RYKALIN, NIKOLAJ: *Berechnung der Wärmevorgänge beim Schweißen*. Bd. 3. Berlin : Verlag Technik, 1957

[24] CHANG, CHIN-LUNG: *Berechnung der Schmelzbadgeometrie beim Laserstrahlschweißen mit Mehrfokustechnik*. Stuttgart, Universität Stuttgart, Dissertation, 2000

[25] KAARS, JONNY ; MAYR, PETER ; KOPPE, KURT: Simple Transition Resistance Model for Spot Welding Simulation of aluminized AHSS. In: *Mathematical Modeling of Weld Phenoma*. Bd. 11, 2016 — ISBN 978-3-85125-490-7

[26] KAARS, JONNY ; MAYR, PETER ; KOPPE, KURT: Generalized dynamic transition resistance in spot welding of aluminized 22MnB5. In: *Materials and Design* Bd. 106 (2016)

[27] KAARS, JONNY ; MAYR, PETER ; KOPPE, KURT: Dynamic apparent transition resistance data in spot welding of aluminized 22MnB5. In: *Data in Brief* Bd. 8 (2016)